Spectral and Kinetic Characterization of the Michaelis Charge Transfer Complex in Monomeric Sarcosine Oxidase †

ARTICLE *in* BIOCHEMISTRY · JUNE 2006

Impact Factor: 3.02 · DOI: 10.1021/bi0600852 · Source: PubMed

Published in final edited form as:
Biochemistry. 2006 May 16; 45(19): 5985–5992. doi:10.1021/bi0600852.

Spectral and Kinetic Characterization of the Michaelis Charge Transfer Complex in Monomeric Sarcosine Oxidase†

Gouhua Zhao and **Marilyn Schuman Jorns***
Department of Biochemistry and Molecular Biology, Drexel University College of Medicine, Philadelphia, PA 19102

Abstract

Monomeric sarcosine oxidase is a flavoenzyme that catalyzes the oxidation of the methyl group in sarcosine (N-methylglycine). Rapid reaction kinetic studies under anaerobic conditions at pH 8.0 show that the enzyme forms a charge transfer Michaelis complex with sarcosine (E-FAD_{ox}·sarcosine) that exhibits an intense long wavelength absorption band (λ_{max} = 516 nm, ε_{516} =4800 M^{-1} cm^{-1}). Since charge transfer interaction with sarcosine as donor is possible only with the anionic form of the amino acid, the results indicate that the pK_a of enzyme-bound sarcosine must be considerably lower than the free amino acid (pK_a = 10.0). No redox intermediate is detectable during sarcosine oxidation, as judged by the isosbestic spectral course observed for conversion of E-FAD_{ox}·sarcosine to reduced enzyme at 25 or 5 °C. The limiting rate of the reductive half-reaction at 25 °C (140 ± 3 s^{-1}) is slightly faster than turnover (117 ± 3 s^{-1}). The kinetics of formation of the Michaelis charge transfer complex can be directly monitored at 5 °C where the reduction rate is 4.5-fold slower and complex stability is increased 2-fold. The observed rate of complex formation exhibits a hyperbolic dependence on sarcosine concentration with a finite y-intercept, consistent with a mechanism involving formation of an initial complex followed by isomerization to yield a more stable complex. Similar results are obtained for charge transfer complex formation with methylthioacetate. The observed kinetics are consistent with structural studies which show that a conformational change occurs upon binding of methylthioacetate and other competitive inhibitors.

Monomeric sarcosine oxidase (MSOX)[1] catalyzes the oxidation of the methyl group in sarcosine (N-methylglycine) to yield glycine, formaldehyde and hydrogen peroxide. The enzyme also catalyzes the oxidation of the equivalent C-N bond in other secondary amino acids, such as L-proline. Sarcosine is a common soil metabolite that can act as sole source of carbon and energy for many microorganisms. MSOX is expressed as an inducible enzyme in many soil bacteria upon growth with sarcosine as source of carbon and energy. The enzyme is a flavoprotein that contains covalently bound FAD [8a-(S-cysteinyl)FAD] (1–7). The crystal structure of free MSOX from *Bacillus sp. B-0618* and complexes of the enzyme with various inhibitors have been determined (2,6,8,9). MSOX is a two-domain, 44 KDa protein. The flavin is bound in an extended conformation with its ADP moiety bound to the flavin domain. The flavin ring is bound at the bottom of a cleft between the flavin and catalytic domains.

MSOX is a member of a growing family of prokaryotic and eukaryotic enzymes that contain covalently bound flavin and catalyze similar oxidation reactions with different amine substrates (10–13). Despite considerable attention, important questions regarding the mechanism of

†This work was supported in part by Grant GM 31704 (M. S. J.) from the National Institutes of Health.

*To whom correspondence should be addressed. Phone: (215) 762-7495 FAX: (215) 762-4452. E-mail: marilyn.jorns@drexelmed.edu.

[1]Abbreviations: MSOX, monomeric sarcosine oxidase; FAD, flavin adenine dinucleotide; SET, single electron transfer; MTA, methylthioacetate; CPG, N-(cyclopropyl)glycine.

flavin-dependent amine oxidation reactions remain unresolved. Postulated mechanisms differ with respect to the involvement of a redox intermediate, the requirement for an active site base and the identity of the acceptor of the α-hydrogen removed from the carbon atom in the C-N bond undergoing oxidation (Scheme 1). There are no redox intermediates in the hydride transfer mechanism where flavin N(5) acts as the acceptor of the α-hydrogen in a reaction that does not require an active site base. In single electron transfer (SET) mechanisms, a flavin radical intermediate is generated by the transfer of an electron from the substrate amino group (14). Polar mechanisms involve formation of a covalent flavin-substrate intermediate in a reversible reaction involving nucleophilic addition of the substrate amino group at flavin C(4a) (15). An active site base is required for the versions of the SET and polar mechanisms shown in Scheme 1 but base-independent variants have been suggested where the α-hydrogen is transferred to flavin N(5) as a hydrogen atom (16) or proton (17), respectively.

The mechanism of amine oxidation by MSOX has been investigated in studies with L-proline, a slow substrate where turnover occurs at less than 1% of the rate observed with sarcosine. Flavin reduction by L-proline is rate-limiting and can be monitored in manual mixing experiments. These studies show that MSOX binds the L-proline zwitterion (pK_a = 10.6) and induces a large decrease in the pK_a of the bound amino acid (ΔpK_a = 2.6). The enzyme·substrate complex exhibits an intense long wavelength absorption band (λ_{max} = 512 nm, ε_{512} = 6800 M^{-1} cm^{-1}, pH 8.6) that is attributable to charge transfer interaction between oxidized FAD and the electron-rich L-proline anion. No redox intermediates are detectable during conversion of this complex to the reduced enzyme·product complex (5–7).

As discussed by Cleland (18), a slow substrate like L-proline can provide a number of advantages in kinetic studies. However, it is clearly important that results obtained with a poor substrate be evaluated in studies with the physiological substrate. In this paper, the reaction of MSOX with sarcosine has been studied by monitoring the reductive half-reaction in rapid reaction kinetic studies. The enzyme·sarcosine complex is readily detectable using this technique. Its spectral properties and the kinetics of both its formation and conversion to reduced enzyme are described.

EXPERIMENTAL PROCEDURES

Materials

Sarcosine and methylthioacetate were purchased from Aldrich. Glucose oxidase and catalase were obtained from Sigma.

Enzyme Purification and Assay

MSOX was were purified as previously described (4). During purification, enzyme activity was measured using the Nash assay and protein was determined using the Bio-Rad micro protein assay. The concentration of purified enzyme was determined based on its absorbance at 454 nm (ε_{454} = 12,200 M^{-1} cm^{-1}) (4).

Spectroscopy

Absorption spectra were recorded using an Agilent Technologies 8453 diode array or a Perkin-Elmer Lambda 2S spectrophotometer.

Rapid Reaction Kinetics

Rapid reaction kinetic measurements were performed by using a Hi-Tech Scientific SF-61DX2 stopped-flow spectrophotometer with diode array or photomultiplier detection, as indicated. Data were collected in log mode to maximize the number of points acquired during the early phase of each reaction. All spectra or single wavelength kinetic traces are averages of at least

five replicate shots. For anaerobic experiments, solutions containing MSOX or sarcosine were prepared in buffer containing 50 mM glucose. The solutions were made anaerobic by multiple cycles of evacuation, followed by flushing with oxygen-scrubbed argon. Glucose oxidase (0.4 U/mL) was then tipped from a side arm of the tonometer to remove traces of residual oxygen and maintain anaerobic conditions. Inclusion of glucose/glucose oxidase eliminated a slow phase that accounted for ~10% of the spectral change observed in initial reductive half-reaction studies. The entire flow circuit of the stopped flow spectrometer was made anaerobic by an overnight incubation with anaerobic buffer containing 50 mM glucose and 0.4 U/mL glucose oxidase. Alternatively, the system was made anaerobic by an overnight incubation with anaerobic buffer containing dithionite (5 mg/mL) and then flushed with anaerobic buffer.

Data Analysis

Global analyses of absorption spectra, acquired by using the stopped-flow instrument with diode array detection, were conducted using Specfit 3.0. This software package performs global least squares fitting by the Levenberg-Marquardt method, evaluation of rate constants and prediction of spectra for transient intermediates. All other data analyses, including fitting of single wavelength kinetic traces, were conducted by using the curve fit function in Sigma Plot (SPSS, Inc.). Spectra corresponding to 100% complex formation were calculated by using observed dissociation constants and spectra recorded for the free enzyme and at the highest ligand concentration tested. The percent complex formation at the highest ligand concentration tested was determined based on the observed dissociation constant. This value and the corresponding observed difference spectrum were used to calculate the difference spectrum for 100% complex formation. The latter was combined with the observed spectrum of the free enzyme to generate the absorption spectrum for 100% complex formation. The positions of charge transfer bands were estimated from difference spectra.

RESULTS

Anaerobic half-reaction of MSOX with sarcosine at 25 °C

A stopped-flow spectrophotometer was used to monitor the reaction of MSOX with various concentrations of sarcosine (1–50 mM) under anaerobic conditions at pH 8.0. At the lower substrate concentrations reduction of the enzyme is slow enough such that virtually the entire spectral course of the reaction can be observed by using the instrument in diode array mode. This is illustrated in Figure 1 by results obtained with 2.5 mM sarcosine, as shown by the black curves. The data provide no evidence for a *redox* intermediate, as judged by the observed isosbestic conversion of oxidized to 2-electron reduced enzyme. Nevertheless, the initial spectrum recorded after mixing differs from that observed in the absence of sarcosine (Figure 1, red curve), especially as regards the development of absorbance in the long wavelength region ($\lambda > 500$ nm). This disparity becomes even more apparent at higher sarcosine concentrations, as shown by the spectral course of the reaction with 50 mM sarcosine (Figure 2). Owing to the much faster reaction rate, the initial part of the reaction at the higher substrate concentration occurs during mixing. Nevertheless, the dramatic increase in long wavelength absorption is apparent in the spectrum obtained immediately after mixing.

The loss of oxidized flavin, as monitored by the decrease in absorbance at 454 nm, exhibits apparent first-order kinetics, as judged by the single exponential fits obtained at all substrate concentrations tested. Apparent first-order kinetics are also found for the disappearance of the long wavelength absorption band, as monitored at 516 nm at sarcosine concentrations above 2.5 mM when the observed absorbance changes are large enough to permit analysis. Similar values are obtained for the rate of oxidized flavin disappearance at 454 nm or the loss of long wavelength absorption at 516 nm, as illustrated by results observed for the reaction with 15 mM sarcosine (k_{obs} = 67.7 ± 0.2 or 69.1 ± 0.2 s^{-1}, respectively) (Figure 3).

Analysis of reaction traces at 454 and 516 nm suggested that an enzyme·substrate complex ($EFAD_{ox}$·S) is formed within the instrument dead time and exhibits a long wavelength absorption band due to charge transfer interaction between oxidized FAD and sarcosine. Conversion of this complex to reduced enzyme ($EFAD_{red}$·P) results in the concomitant loss of absorption due to oxidized flavin and the charge transfer interaction. To evaluate this hypothesis, the data were analyzed globally by fitting observed spectra (300 to 700 nm) to a simple A → B → C model using SpecFit software. An excellent correlation is found between rates of enzyme reduction estimated by global analysis (B → C) and values obtained by single wavelength analysis (Figure 4, inset). The observed apparent first-order rate constants (k_{obs}) exhibit a hyperbolic dependence on sarcosine concentration (Figure 4). The corresponding double-reciprocal plot is linear with a finite Y-intercept (plot not shown). The results are consistent with a mechanism involving a rapidly attained equilibrium (K_d) between free MSOX and the enzyme·sarcosine charge transfer complex, followed by an essentially irreversible flavin reduction step (k_{lim}) (Scheme 2). Values for the limiting rate of reduction at saturating sarcosine and the apparent dissociation constant of the charge transfer complex were estimated by fitting the data to eq. 1.

$$k_{obs}=k_{lim}[\text{sarcosine}]/(K_d+[\text{sarcosine}]) \quad (1)$$

The value obtained for k_{lim} ($140 \pm 3\ s^{-1}$) is just slightly larger than a value previously obtained for k_{cat} in steady-state kinetic studies ($k_{cat} = 117 \pm 3\ s^{-1}$) at 25 °C (3). This outcome suggests that the reductive half-reaction is at least partly rate-limiting during turnover. The value obtained for the apparent K_d for sarcosine is similar to value that obtained for the K_m (Table 1).

In addition to estimating rate constants, global fitting of diode array data to the model, A → B → C, also generates calculated spectra for the mixture of free enzyme and the enzyme·sarcosine complex (B) at each substrate concentration. The calculated spectra are virtually isosbestic and show the progressive formation of an intense charge transfer band as the substrate concentration is increased (Figure 5). The charge transfer absorption band exhibits a maximum at 516 nm, as estimated based on the position of the peak in the difference spectrum (data not shown). A dissociation constant for the complex was calculated by fitting a theoretical binding curve to the observed absorbance changes at 516 nm (Figure 5, inset). The value obtained by this approach ($K_d = 13 \pm 1$ mM) agrees well with the value estimated from reduction rates (Table 1). The extinction coefficient of the charge transfer complex at 516 nm ($\varepsilon = 4800\ M^{-1}\ cm^{-1}$) was determined based on the absorption spectrum calculated for 100% complex formation.

Diode Array Analysis of the Anaerobic Half-reaction of MSOX with Sarcosine at 5 °C

The tail end of charge transfer complex formation is detectable at 5 ° C, as judged by the initial few spectra collected in diode array mode, but the reactions were too fast to monitor appropriately using this technique. Except for this difference, the spectral course of the reactions at 5 °C were very similar to that observed at 25 °C. Rate constants for enzyme reduction (B → C) at 5 °C were obtained by global fitting of the data to a simple A → B → C model. The observed reduction rates exhibit a hyperbolic dependence on the concentration of sarcosine (Figure 4) and the corresponding double-reciprocal plot is linear with a finite Y-intercept, similar to results obtained at 25 °C. The limiting rate of the reaction at 5 °C ($k_{lim} = 31.1 \pm 0.1\ s^{-1}$) is 4.5-fold slower and sarcosine binding is about 2-fold tighter ($K_d = 6.4 \pm 0.1$ mM) than observed at 25 °C (Table 1). The properties the MSOX·sarcosine charge transfer complex at 5 °C were further evaluated based on spectra calculated by global analysis of data at each substrate concentration. The K_d estimated by this method ($K_d = 7.3 \pm 0.2$ mM) is in good agreement with the value obtained from reduction rates. The spectral properties obtained

for the charge transfer complex at 5 °C (λ_{max} = 515 nm; ε_{515} = 4700 M^{-1} cm^{-1}) are very similar to those observed at 25 °C (λ_{max} = 516 nm; ε_{516} = 4800 M^{-1} cm^{-1}).

Kinetics of Formation of the MSOX·Sarcosine Charge Transfer Complex at 5 °C

The diode array studies at 5 °C suggested that sufficient data for kinetic analysis might be obtained by monitoring the formation and decay of the charge transfer band at a single wavelength. Accordingly, studies were conducted using a range of sarcosine concentrations (2.5 to 80 mM) and monitored at 516 nm in photomultiplier mode at 5 °C. In addition, a 5-fold higher enzyme concentration (93.8 μM) was used in order to maximize the observed absorbance change. This was especially helpful at the highest substrate concentrations tested where the observed rates of complex formation approach the limit of the stopped flow spectrometer. Under these conditions, reaction traces obtained at all substrate concentrations tested gave an excellent fit to a double exponential equation ($y = Ae^{-kat} + Be^{-kbt} + C$) where k_a and k_b are apparent first order rate constants for the formation and decay of the charge transfer complex (Figure 6).

Values for the rate of complex disappearance (k_b) exhibit a hyperbolic dependence on the sarcosine concentration (Figure 6, inset); the corresponding double-reciprocal plot is linear with a finite Y-intercept (plot not shown). Values estimated for the limiting rate of reduction (k_{lim} = 38.0 ± 0.3 s^{-1}) and the dissociation constant of the charge transfer complex (K_d = 14.3 ± 0.3 min^{-1}) based on spectral changes at 516 nm are in fairly good agreement with those obtained by global analysis of the diode array data (Table 1).

Since enzyme reduction is much slower, it was anticipated that the observed rate of charge transfer complex formation (k_a) would correspond to a simple approach to equilibrium and exhibit a linear dependence on substrate concentration. Instead, values obtained for k_a were found to approach a limiting value at high sarcosine concentrations (Figure 7); the corresponding double reciprocal plot is not linear (plot not shown). This behavior is indicative of a mechanism involving a two-step equilibrium process where formation of an initial enzyme-substrate complex is followed by an isomerization reaction to yield a more stable complex (Scheme 3)

$$k_{obs} = \frac{k_3[S]}{[S] + k_2/k_1} + k_4 \quad (2)$$

(19,20). According to this mechanism, the observed rate of formation of the stable complex should exhibit a hyperbolic dependence on ligand concentration *and* a finite value (k_4) for the y-intercept (equation 2).

Indeed, a good fit to equation 2 was obtained for the observed rate of charge transfer complex formation at all sarcosine concentrations tested (Figure 7). This analysis yields values for k_3 (1010 ± 40 s^{-1}), k_4 (190 ± 20 s^{-1}) and the microscopic K_d for the primary binding step (k_2/k_1 = 29

$$K_{d(macroscopic)} = \frac{k_2 k_4}{k_1 k_3}\left(\frac{1}{1 + k_4/k_3}\right) \quad (3)$$

± 4 mM). The overall macroscopic dissociation constant was calculated using these parameters and equation 3. The calculated value (K_d = 4.6 ± 0.3 mM) is in good agreement with the value estimated based on global analysis of the diode array data (K_d = 6.4 ± 0.1 mM) (Table 2).

Kinetics of Formation of a MSOX·Inhibitor Charge Transfer Complex at 5 °C

In addition to substrate, MSOX forms charge transfer complexes with various inhibitors, including methylthioacetate (MTA) (2,6,8). This compound acts as a competitive inhibitor and forms a complex with MSOX that exhibits an intense charge transfer band at 532 nm. MTA is a sarcosine analog where the substrate nitrogen is replaced by sulfur. Unlike sarcosine, MTA does not exist as a zwitterion that must undergo loss of a proton in order to act a charge transfer donor at neutral pH. This feature and the fact that MTA forms a redox-inactive dead end complex suggested that the kinetics of complex formation with MTA could provide a useful benchmark for comparison with results obtained for the Michaelis complex. A static spectrophotometric titration showed that the MSOX·MTA charge transfer complex is nearly 6-fold more stable at 5° C (K_d = 0.50 ± 0.02 mM) but exhibits spectral properties (Figure 8, inset) similar to those observed in previous studies at 25 °C (K_d = 2.88 ± 0.04 mM) (6). The kinetics of complex formation at 5° C were monitored by following the increase in absorption at 532 nm at MTA concentrations from 1 to 45 mM. The traces gave a good fit to a double exponential equation ($y = Ae^{-kobst} + Be^{-kob2t} + C$) with ~95% of the absorbance change occurring at an observed rate (k_{obs}) that varied depending on the concentration of MTA. Values for k_{obs} exhibit a hyperbolic dependence on MTA concentration and gave a good fit to equation 2 (k_3 = 2450 ± 150 s^{-1}, k_4 = 18 ± 5 s^{-1}, k_2/k_1 = 87 ± 8) (Figure 9), similar to that observed with sarcosine. The macroscopic dissociation constant for the MSOX·MTA complex was calculated using these parameters and equation 3. The calculated value (K_d = 0.63 ± 0.08 mM) is in good agreement with that obtained from the static spectrophotometric titration (Table 2). A small portion (~5%) of the spectral change observed with MTA occurred in a second phase at a rate that was independent of the ligand concentration (k_{obs2} = 39 ± 3 s^{-1}). The origin of this effect is unclear. A comparable feature would be difficult to detect with the Michaelis complex owing to the ensuing redox reaction.

DISCUSSION

Reaction of MSOX with sarcosine at pH 8.0 results in the formation an enzyme·substrate complex that exhibits an intense long wavelength absorption band. The long wavelength absorption is attributable to the formation of an enzyme·substrate complex with oxidized FAD and sarcosine acting as charge transfer acceptor and donor, respectively. The zwitterionic form of sarcosine is the predominant species in solution at pH 8.0 (pK_a = 10.0). Charge transfer interaction with sarcosine as donor is possible only with the anionic form of the substrate. The results indicate that the pK_a of MSOX-bound sarcosine must be considerably lower than the free amino acid, as observed with L-proline (5). The position and intensity of the charge transfer band observed for the complex of MSOX with its physiological substrate (λ_{max} = 516 nm, ε_{516} = 4800 M^{-1} cm^{-1}) resemble that seen for the complex with L-proline (λ_{max} = 512 nm, ε_{512} = 6800 M^{-1} cm^{-1}, pH 8.6) (7). It is generally agreed that the unprotonated amine is the reactive species in flavin-dependent amine oxidation reactions. The results suggest that both sarcosine and L-proline are activated for MSOX oxidation by a process involving stabilization of the reactive anionic form.

No evidence was obtained for the formation of a redox intermediate during sarcosine oxidation, as judged by the observed isosbestic conversion of the enzyme·substrate charge transfer complex to reduced enzyme. Similar results are seen with the poor substrate, L-proline (3,5). While the data with both substrates are consistent with a hydride transfer mechanism they cannot be used to rule out a SET or polar mechanism because a radical or 4a-adduct

intermediate might be formed in small amounts that are difficult to detect. Model studies show that a relatively stable 4a-adduct is formed upon reaction of cyclopropylamines with a flavin derivative activated towards nucleophilic addition at C(4a) (15). A 4a-adduct is, however, not observed upon reaction of MSOX with N-(cyclopropyl)glycine (CPG) (9,21). Instead, CPG forms a complex with MSOX that exhibits a charge transfer band (λ_{max} = 519 nm, ε_{519} = 4800 M^{-1} cm^{-1}, pH 8.0) (9) similar to that observed with sarcosine or L-proline. Unlike normal substrates, CPG acts as a mechanism-based inactivator of MSOX. Inactivation results in the formation of a modified reduced flavin, accompanied by cleavage of the cyclopropyl ring of CPG (9). Although CPG inactivation of MSOX occurs via a SET mechanism, the inactivation rate is ~10^5-fold slower than enzyme reduction by sarcosine. The results suggest that a radical mechanism can be forced by the use of a highly reactive substrate analog but is unlikely to account for the reaction of MSOX with its physiological substrate.

The kinetics observed for formation of a charge transfer complex between MSOX and sarcosine or MTA are indicative of a mechanism involving formation of an initial complex, (ES)*, followed by isomerization to yield a more stable complex. The results suggest that a conformational change is triggered upon ligand binding, consistent with changes observed in the crystal structure of MSOX upon binding of MTA (Figure 10) and other carboxylate-containing ligands (2, 8). In each case, the carboxylate group forms hydrogen bonds with the ε-amino group of Lys348 and the guanidinum side chain of Arg52. Although the position of Lys348 is unchanged, ligand binding does result in the movement of Arg52 into the active site and the displacement of all but two of the water molecules that are bound at the active site in free MSOX. A loop (Gly56 to Glu60) that forms part of the cleft leading from the surface to the active site is found in a closed conformation in these complexes where it blocks access of bulk solvent to the active site (Figure 10, top panel). The active site loop appears to be mobile in the free enzyme and can assume either the open or closed configuration (see (6) and PDB code 1L9F). Conversion from the open to the closed form is accompanied by a decrease in the number of active site water molecules from nine to seven (Figure 10, bottom panel). In the open form, five waters occupy the ligand binding site above the *re*-face of the flavin and two waters are bound near Arg52. One less water is found in each of these locations in the closed form. Both forms contain two additional waters that form hydrogen bonds to FAD N(5) (WAT 1) and His269:NE2 (WAT 6), respectively, and are retained in MSOX·ligand complexes (Figure 10, bottom panel). We speculate that formation of the initial complex, (E-S)*, involves binding of the ligand to the open form of the enzyme in a process driven by electrostatic interaction of the ligand carboxylate with Lys348 and accompanied by the displacement of five active site water molecules (Figure 10, bottom panel, WAT 2, 3′, 3″,4 5). Formation of an analogous salt bridge is proposed as a key driving force in the initial binding of ligands to lactate dehydrogenase and triosephosphate isomerase (22, 23). We postulate that the ligand carboxylate in the initial MSOX complex “recruits” Arg52 in a process that results in the displacement of the two waters near Arg52 (Figure 10, bottom panel, WAT 7, 8) and conversion to a more stable closed complex. Kinetic and thermodynamic studies indicate that MSOX binds the zwitterionic form of L-proline (5, 7). Substrate ionization may be promoted by hydrogen bond and electrostatic interactions at the active site that stabilize the anion. For example, a strong hydrogen bond is probably formed between the substrate amino group and the backbone carbonyl of gly344, as judged by results obtained with suitable analogs (e.g., pyrrole-2-carboxylate, dimethylglycine) (2, 8). The active site environment of MSOX is highly electropositive. There are no acidic residues near the flavin ring, a region that does include a number of basic residues (Lys348, Arg52, Arg49, Lys265) that might help to stabilize the substrate anion. According to this scenario, substrate ionization might occur during conversion of (E-S)* to the more stable complex. A putative proton relay system, located adjacent to the *si*-face of the flavin ring (7), may provide a path for proton release to bulk solvent.

Acknowledgments

We thank Drs. F. Scott Mathews, Patrick Loll and David Ballou for helpful discussions.

References

1. Kvalnes-Krick, K.; Jorns, MS. Role of the covalent and noncovalent flavins in sarcosine oxidase. In: Muller, F., editor. Chemistry and Biochemistry of Flavoenzymes. CRC Press Inc.; Boca Raton: 1991. p. 425-435.
2. Wagner MA, Trickey P, Chen Z, Mathews FS, Jorns MS. Monomeric sarcosine oxidase: 1. Flavin reactivity and active site binding determinants. Biochemistry 2000;39:8813–8824. [PubMed: 10913292]
3. Wagner MA, Jorns MS. Monomeric sarcosine oxidase: 2. Kinetic studies with sarcosine, alternate substrates and substrate analogs. Biochemistry 2000;39:8825–8829. [PubMed: 10913293]
4. Wagner MA, Khanna P, Jorns MS. Structure of the flavocoenzyme of two homologous amine oxidases: Monomeric sarcosine oxidase and N-methyltryptophan oxidase. Biochemistry 1999;38:5588–5595. [PubMed: 10220347]
5. Zhao G, Jorns MS. Monomeric sarcosine oxidase: Evidence for an ionizable group in the ES complex. Biochemistry 2002;41:9747–9750. [PubMed: 12146940]
6. Zhao G, Song H, Chen Z, Mathews FS, Jorns MS. Monomeric sarcosine oxidase: Role of histidine 269 in catalysis. Biochemistry 2002;41:9751–9764. [PubMed: 12146941]
7. Zhao G, Jorns MS. Ionization of zwitterionic amine substrates bound to monomeric sarcosine oxidase. Biochemistry 2005;44:16866–16874. [PubMed: 16363800]
8. Trickey P, Wagner MA, Jorns MS, Mathews FS. Monomeric sarcosine oxidase: Structure of a covalently-flavinylated secondary amine oxidizing enzyme. Structure 1999;7:331–345. [PubMed: 10368302]
9. Chen Z, Zhao G, Martinovic S, Jorns MS, Mathews FS. Structure of the sodium borohydride-reduced N-(cyclopropyl)glycine adduct of the flavoenzyme monomeric sarcosine oxidase. Biochemistry 2005;44:15444–15450. [PubMed: 16300392]
10. Khanna P, Jorns MS. Characterization of the FAD-containing N-methyltryptophan oxidase from *Escherichia coli*. Biochemistry 2001;40:1441–1450. [PubMed: 11170472]
11. Venci D, Zhao G, Jorns MS. Molecular characterization of nikD, a new flavoenzyme important in the biosynthesis of nikkomycin antibiotics. Biochemistry 2002;41:15795–15802. [PubMed: 12501208]
12. Eschenbrenner M, Chlumsky LJ, Khanna P, Strasser F, Jorns MS. Organization of the multiple coenzymes and subunits and role of the covalent flavin link in the complex heterotetrameric sarcosine oxidase. Biochemistry 2001;40:5352–5367. [PubMed: 11330998]
13. Dodt G, Kim DG, Reimann SA, Reuber BE, McCabe K, Gould SJ, Mihalik SJ. L-pipecolic acid oxidase, a human enzyme essential for the degradation of L-pipecolic acid, is most similar to the monomeric sarcosine oxidases. Biochem J 2000;345:487–494. [PubMed: 10642506]
14. Silverman RB. Radical ideas about monoamine oxidase. Acc Chem Res 1995;28:335–342.
15. Kim JM, Hoegy SE, Mariano PS. Flavin chemical models for monoamine oxidase inactivation by cyclopropylamines, alpha-silylamines, and hydrazines. J Am Chem Soc 1995;117:100–105.
16. Silverman RB, Zelechonok Y. Evidence for a hydrogen atom transfer mechanism or a proton fast electron transfer mechanism for monoamine oxidase. J Org Chem 1992;57:6373–6374.
17. Miller JR, Edmondson DE. Structure-activity relationships in the oxidation of para-substituted benzylamine analogues by recombinant human liver monoamine oxidase A. Biochemistry 1999;38:13670–13683. [PubMed: 10521274]
18. Cleland WW. The use of pH studies to determine chemical mechanisms of enzyme-catalyzed reactions. Methods Enzymol 1982;87:390–405. [PubMed: 7176923]
19. Strickland S, Palmer G, Massey V. Determination of dissociation constants and specific rate constants of enzyme-substrate (or protein-ligand) interactions from rapid reaction kinetic data. J Biol Chem 1975;250:4048–4052. [PubMed: 1126943]

20. Chaiyen P, Brissette P, Ballou DP, Massey V. Thermodynamics and reduction kinetics properties of 2-methyl-3-hydroxypryidine-5-carboxylic acid oxygenase. Biochemistry 1997;36:2612–2621. [PubMed: 9054568]

21. Zhao G, Qu J, Davis FA, Jorns MS. Inactivation of monomeric sarcosine oxidase by reaction with N (cyclopropyl)glycine. Biochemistry 2000;39:14341–14347. [PubMed: 11087383]

22. McClendon S, Zhadin N, Callender R. The approach to the Michaelis complex in lactate dehydrogenase: The substrate binding pathway. Biophys J 2005;89:2024–2032. [PubMed: 15980172]

23. Desamero R, Rozovsky S, Zhadin N, McDermott A, Callender R. Active site loop motion in triosephosphate isomerase: T-jump relaxation spectroscopy of thermal activation. Biochemistry 2003;42:2941–2951. [PubMed: 12627960]

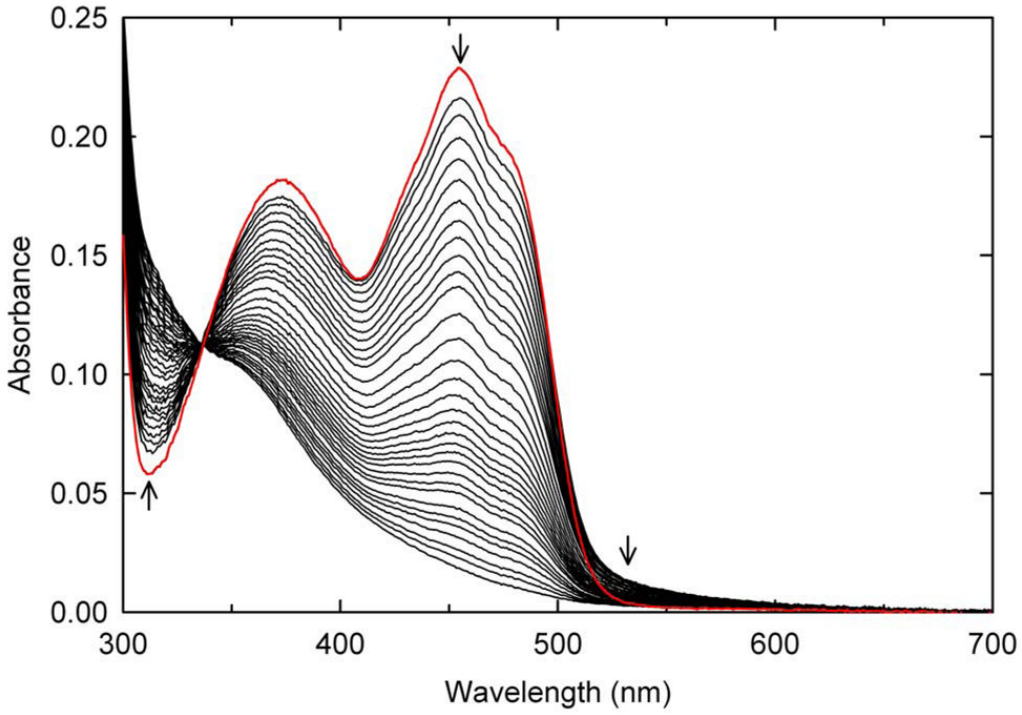

Figure 1.

Spectral course of the anaerobic half-reaction of MSOX with 2.5 mM sarcosine at 25 °C. The black curves show spectra obtained from 1.49 ms to 2.85 s after mixing 18.7 μM MSOX with 2.5 mM sarcosine in 0.1 M potassium phosphate buffer, pH 8.0. Arrows indicate the direction of observed spectral changes. The red curve is the spectrum obtained for free MSOX (18.7 μM) under otherwise identical conditions.

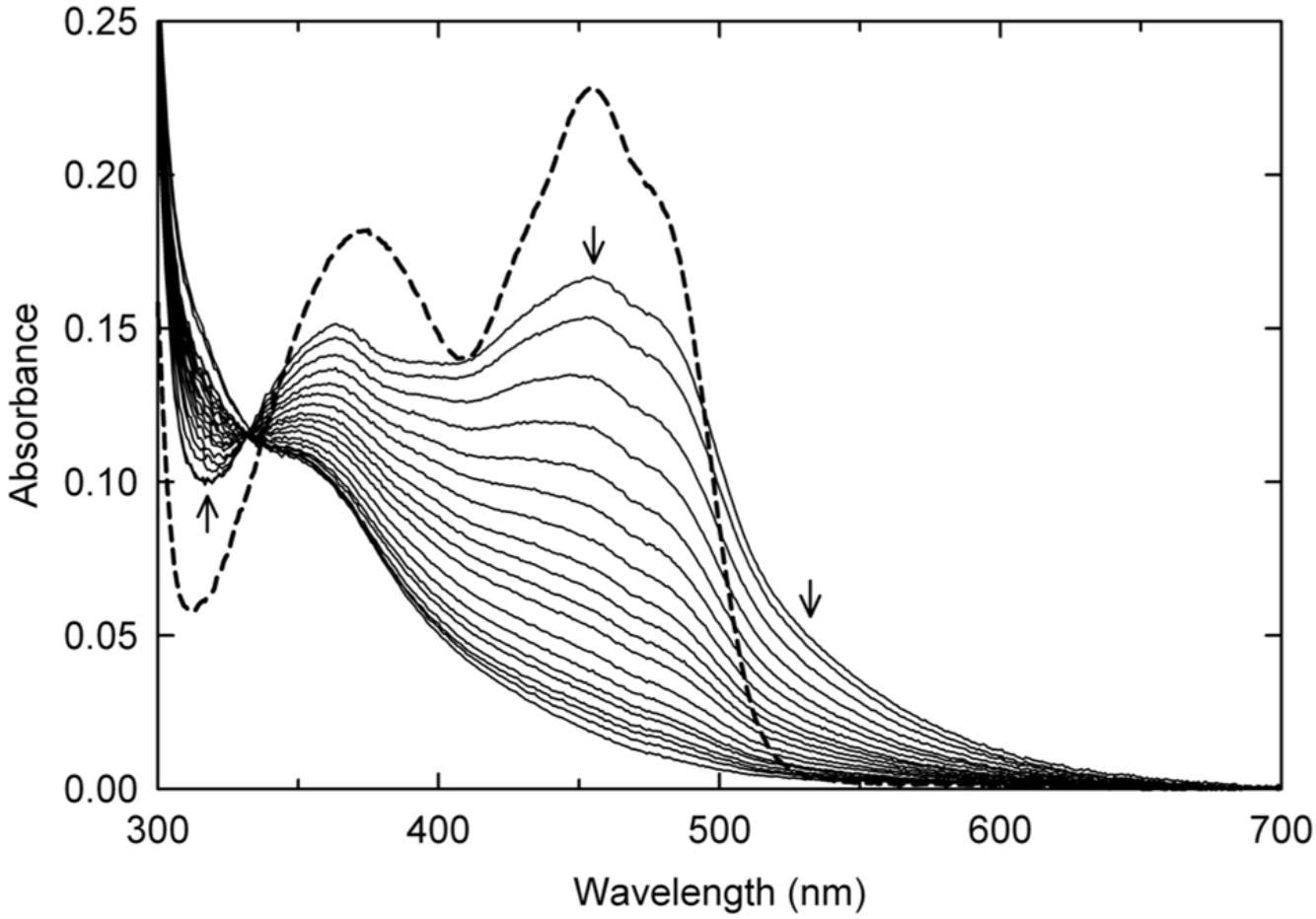

Figure 2.
Spectral course of the anaerobic half-reaction of MSOX with 50 mM sarcosine at 25 °C. The solid black curves show spectra obtained from 0.74 ms to 1.43 s after mixing 18.7 μM MSOX with 50 mM sarcosine in 0.1 M potassium phosphate buffer, pH 8.0. Arrows indicate the direction of observed spectral changes. The dashed black curve is the spectrum obtained for free MSOX (18.7 μM) under otherwise identical conditions.

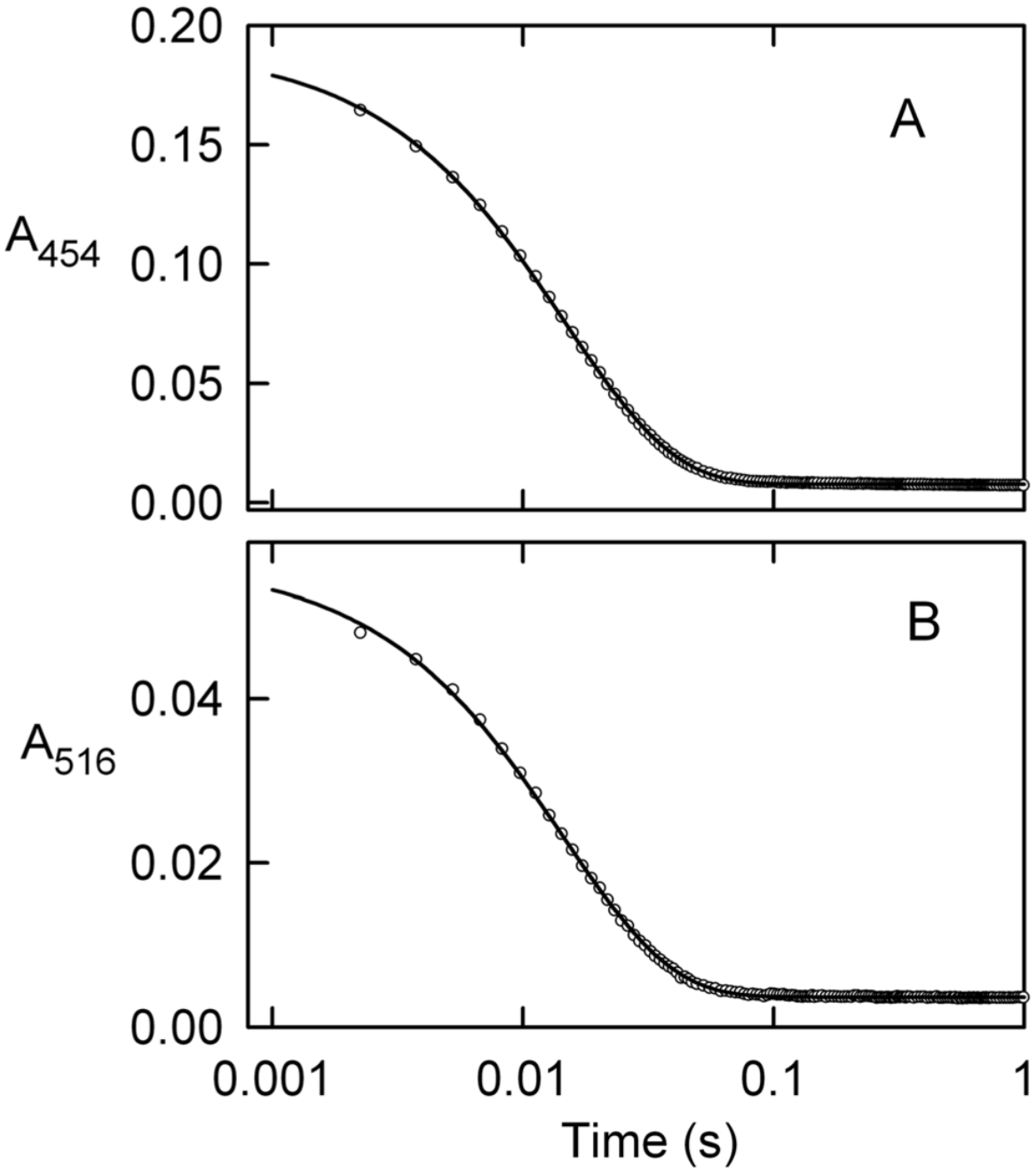

Figure 3.
Kinetics of the anaerobic half-reaction of MSOX with 15 mM sarcosine at 25 °C. Reactions were conducted in 0.1 M potassium phosphate buffer, pH 8.0. Absorbance changes observed at 454 and 516 nm, respectively, are shown in panels A and B, respectively. The solid curves are fits of the data (black circles) to an equation for a single exponential decay ($y = Ae^{-kt} + B$).

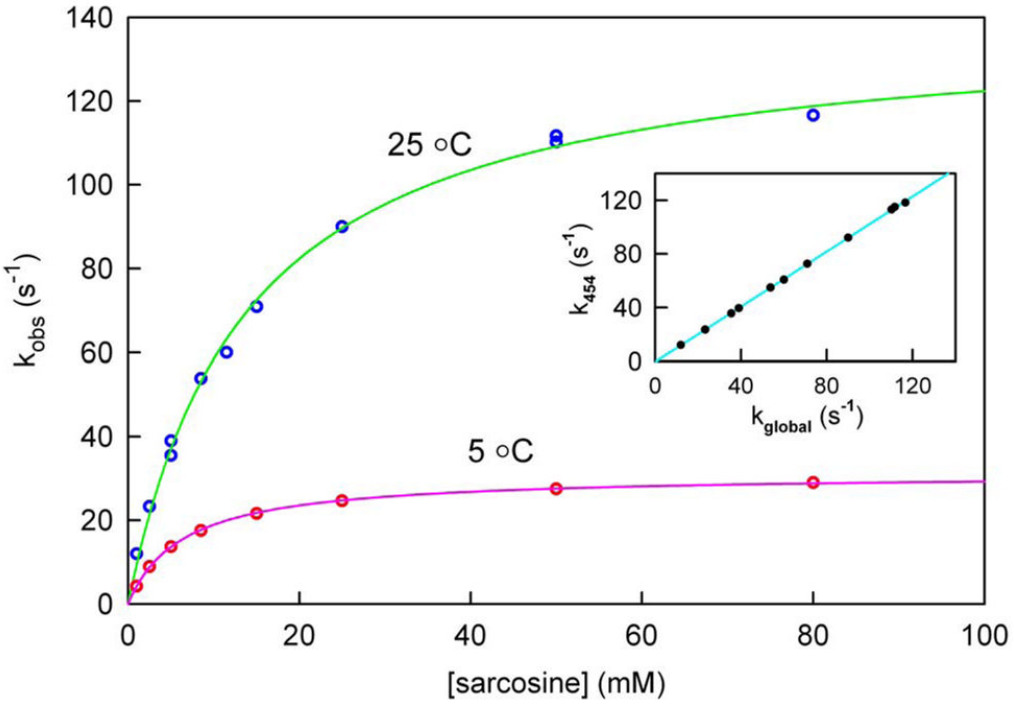

Figure 4.

Effect of sarcosine concentration on the observed rate of the reductive half-reaction. Values for k_{obs} (circles) were obtained by global analysis of diode array stopped-flow data obtained for the reaction of 18.7 or 18.0 μM MSOX with sarcosine in 100 mM potassium phosphate buffer, pH 8.0, at 25 or 5 °C, respectively. The solid lines are fits of the data to equation 1. Inset: Rate constants obtained for enzyme reduction at 25 °C by analysis of absorbance changes at 454 nm (k_{454}) are plotted against values estimated for the same reactions by global analysis (k_{global}) of absorption spectra (300 to 700 nm). The solid line was obtained by linear regression analysis ($r^2 = 0.9998$).

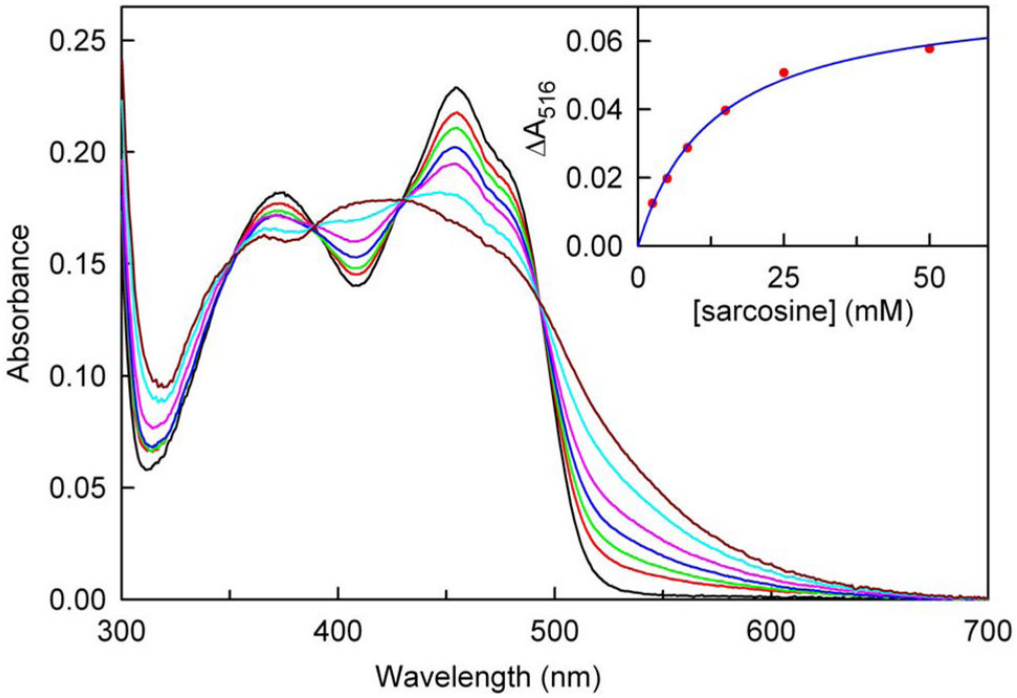

Figure 5.

Calculated absorption spectra for the MSOX·sarcosine charge transfer complex formed at 25 °C. Spectra were calculated by global analysis of the diode array stopped flow data obtained at various sarcosine concentrations, as described in the text. The black curve is the spectrum of free MSOX (18.7 μM). Calculated spectra for the mixture of free E and E·S complex formed with 2.5, 5.0, 8.5, 15, and 50 mM sarcosine are shown by the red, green, blue, magenta and cyan curves, respectively. The brown curve shows the spectrum calculated for 100% complex, as described in Experimental Procedures. The inset shows a plot of the absorbance increase at 516 nm *versus* the sarcosine concentration. The solid line is a fit of a theoretical binding curve to the data (red circles).

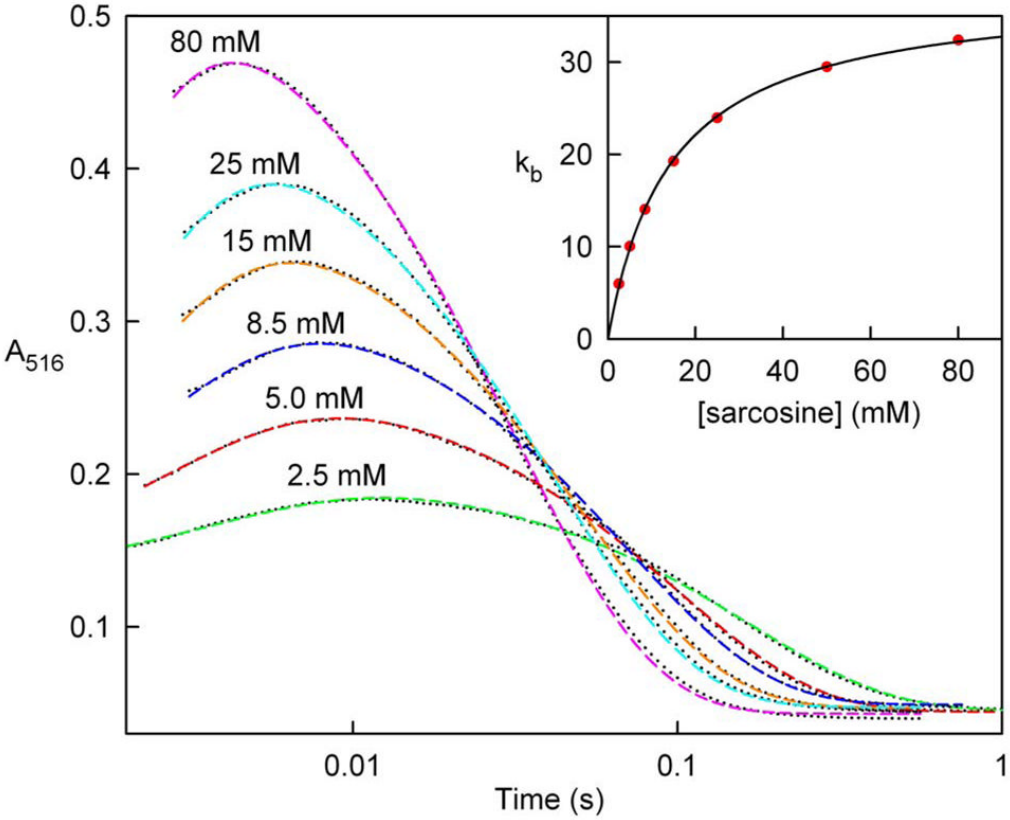

Figure 6.

Kinetics of formation and disappearance of the MSOX·sarcosine charge transfer complex at 5 °C. Reactions were conducted with 93.8 μM MSOX and the indicated sarcosine concentration in anaerobic 100 mM potassium phosphate buffer, pH 8.0, at 5 °C and monitored at 516 nm with the stopped flow spectrometer in photomultiplier mode. The dashed colored curves are fits of the data (black dots) to a double exponential equation ($y = Ae^{-kat} + Be^{-kbt} + C$) where k_a and k_b are apparent first order rate constants for the formation and decay of the charge transfer complex. The inset shows the effect of sarcosine concentration on observed values for k_b (red circles). The solid line is a fit of the data to equation 1.

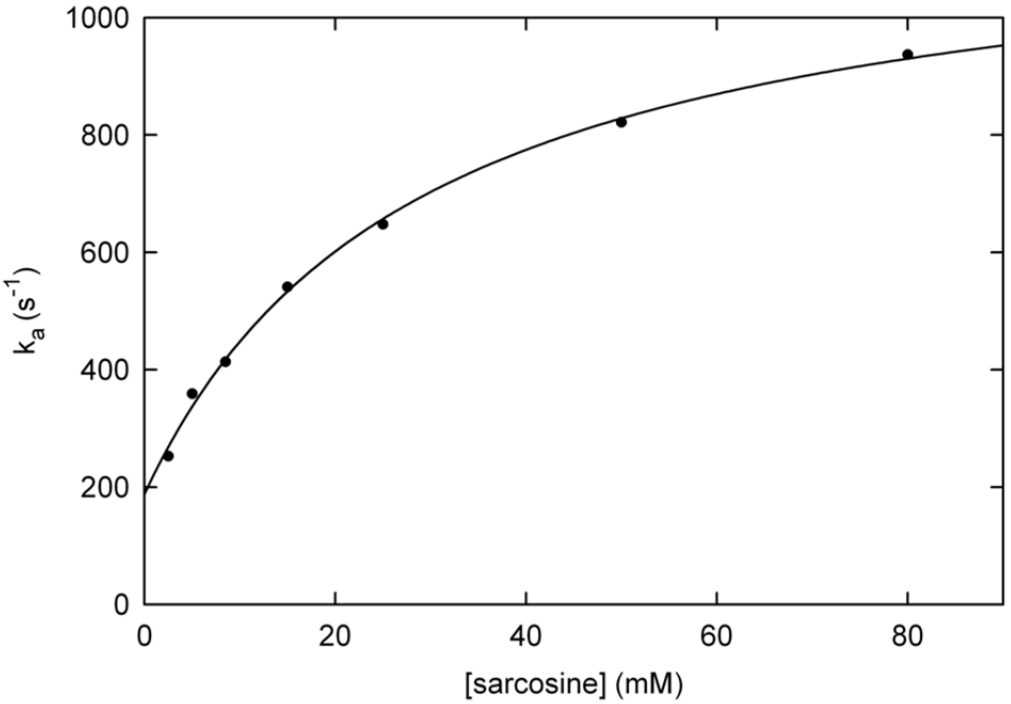

Figure 7.

Effect of sarcosine concentration on the observed rate of formation of the charge transfer complex (k_a) at 5 °C. Values for k_a (black circles) were determined as described in the legend to Figure 6. The solid line is a fit of the data to equation 2.

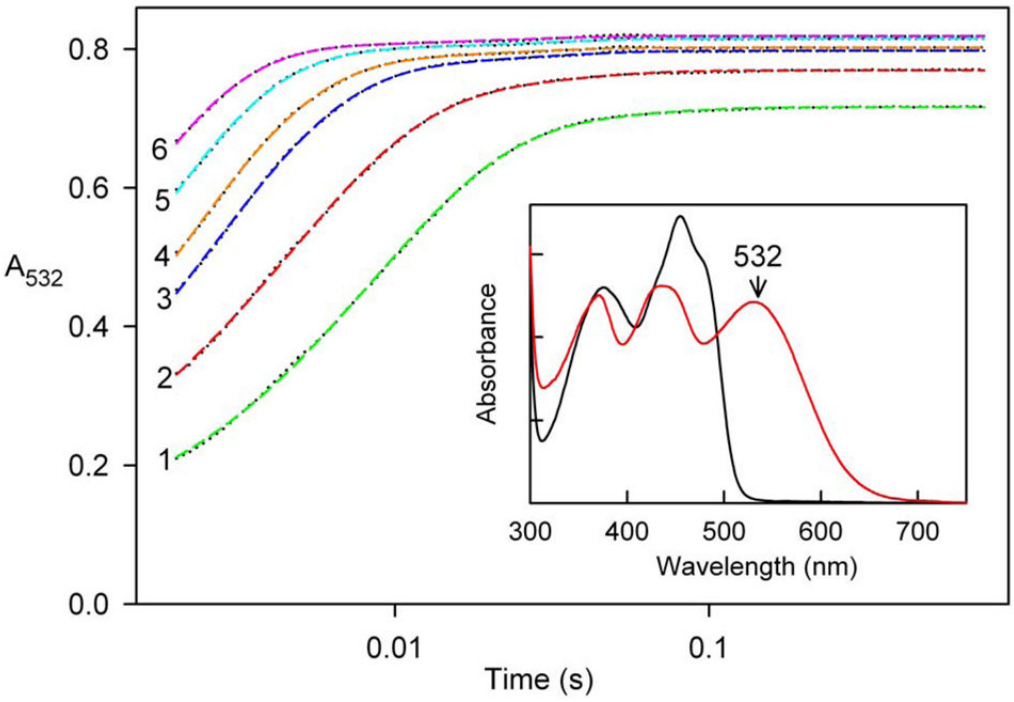

Figure 8.

Kinetics of formation of the MSOX·MTA charge transfer complex at 5 °C. Reactions were conducted in aerobic 100 mM potassium phosphate buffer, pH 8.0, at 5° C with 18 or 90 μM MSOX at MTA concentrations ≤ 16 or ≥ 16 mM, respectively. The observed absorbance changes at 532 nm are normalized to the same enzyme concentration (90 μM). The dashed colored curves are fits of the data (black dots) to a double exponential equation ($y = Ae^{-kobst} + Be^{-kobs2t} + C$). Curves 1 to 6 were obtained with 4, 8, 16, 20, 30 and 45 mM MTA, respectively. (For clarity, reaction traces at additional MTA concentrations are not shown.) Inset: The black curve is the absorption spectrum of free MSOX in 100 mM potassium phosphate buffer, pH 8.0, at 5 °C. The red curve is the spectrum of the MTA complex, calculated for 100% complex formation as described in Experimental Procedures.

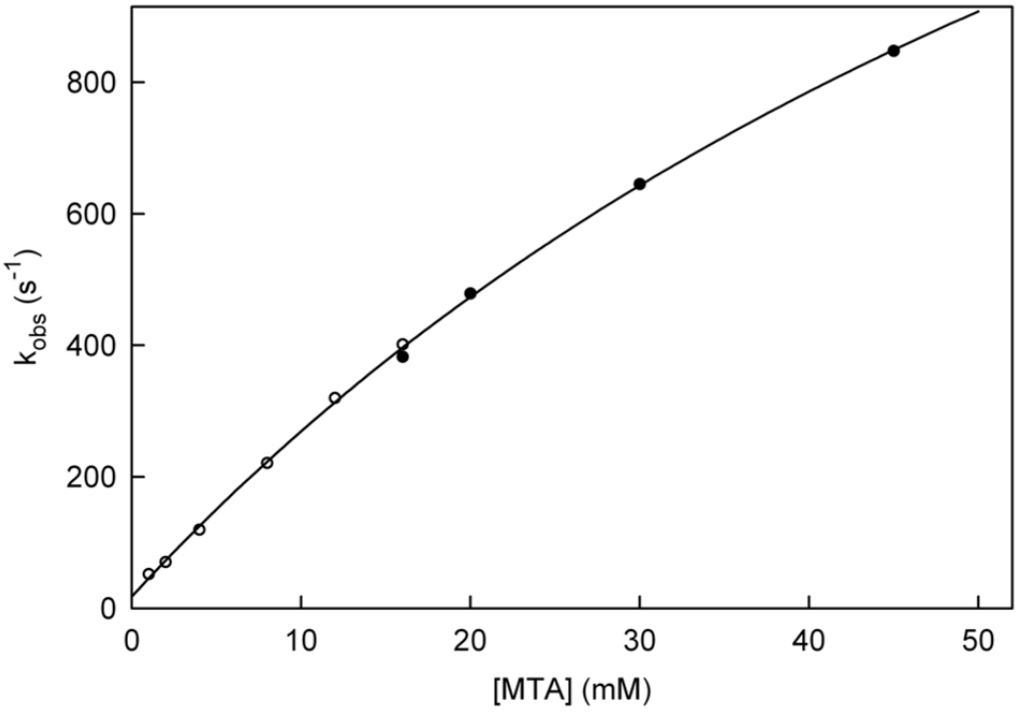

Figure 9.

Effect of MTA concentration of the observed rate of formation of the charge transfer complex at 5 °C. Values for k_{obs} were determined as described in the legend to Figure 8. Data obtained with 18 or 90 μM MSOX are shown by the open or filled circles, respectively. The solid line is a fit of the data to equation 2.

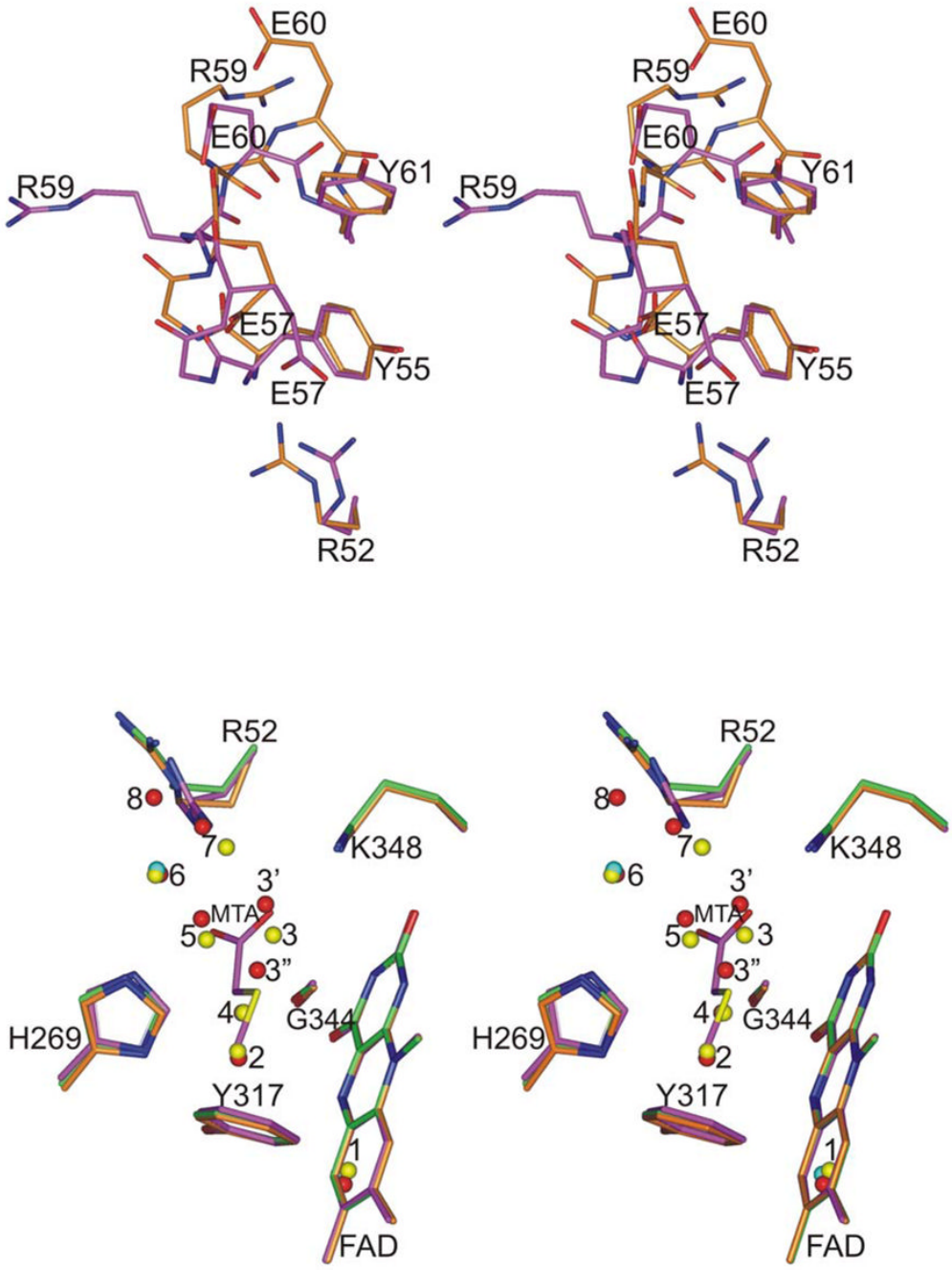

Figure 10.

Conformational changes observed upon binding of MTA. The top panel shows a stereoview of the active site loop and Arg52 in the MSOX complex with MTA (PDB code 1EL9) or in the open conformation of free MSOX (PDB code 1L9F, subunit 1). Carbon atoms are magenta in the MTA complex or gold in the open conformation free MSOX. In both structures, oxygens are red and nitrogens are blue. The bottom panel is a stereoview comparison of the active site in the MTA complex and the open (subunit 1) or closed (subunit 2) conformation of free MSOX (PDB code 2GB0, a revised version of PDB code 1L9F that incorporates a recent refinement of active site waters). Carbon atom colors for the MTA complex (magenta) and the open conformation of free MSOX (gold) are the same as in the top panel; carbon atoms are green

in the closed conformation of free MSOX. Active site waters are shown as balls, colored red for the nine waters in the open form of free MSOX (WAT 1, 2, 3′, 3″, 4–8), yellow for the seven waters in closed form of free MSOX (WAT 1–7) and cyan for the two waters in the MTA complex (WAT 1, 6). (WAT 4 in the open form of free MSOX is largely obscured by WAT 4 in the closed form.) All other oxygens are shown in red. Nitrogens are blue and the sulfur in MTA is shown in yellow.

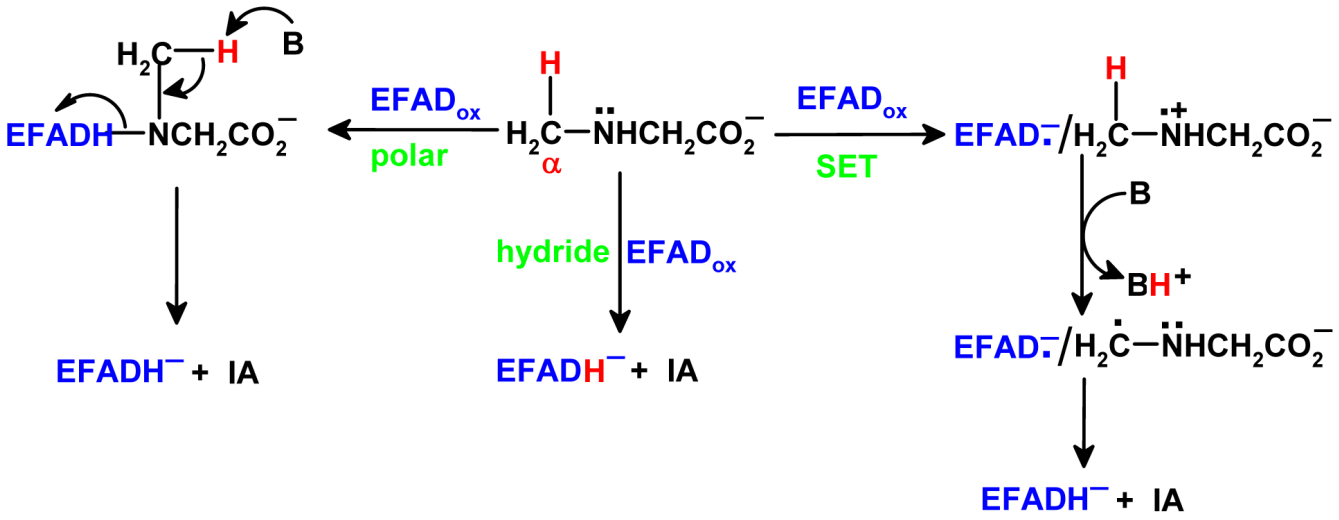

Scheme 1.

Possible mechanisms for sarcosine oxidation by MSOX. IA is the imino acid product of sarcosine oxidation (CH_2=NH^+-CH_2-CO_2^-); $FADH^-$ is the 1,5-dihydroflavin anion. The second electron transfer step in the SET mechanism involves electron transfer from imine radical to flavin radical, accompanied by the transfer of a proton (not shown) to flavin N(5).

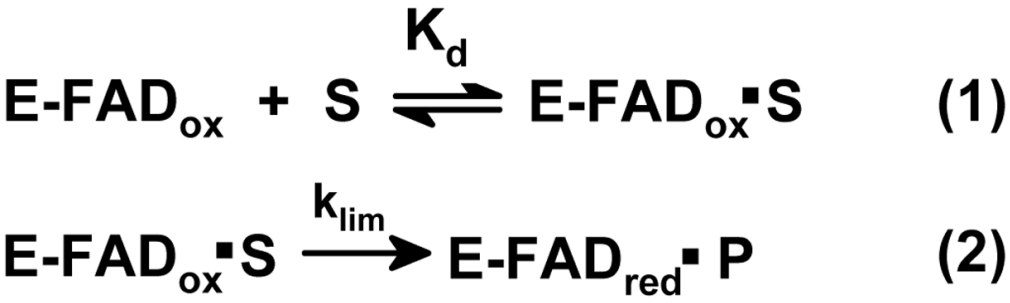

Scheme 2.
Reduction of MSOX by sarcosine by a mechanism involving formation of a transient enzyme·substrate charge transfer complex.

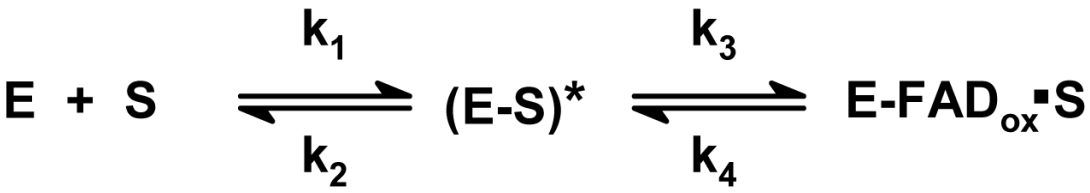

Scheme 3.
Proposed mechanism for charge transfer complex formation.

Table 1

Kinetic parameters for the reductive half-reaction of MSOX with sarcosine at 25 ° or 5 °C or steady-state turnover at 25 °C[a]

Temperature	Reductive-half reaction k_{lim} (s^{-1})	K_d (mM)	Steady-state turnover k_{cat} (s^{-1})	K_m (mM)
25 °C	140 ± 3	13.9 ± 0.7 13.0 ± 1[b]	117 ± 3	9.4 ± 0.4
5 °C	31.1 ± 0.1 38.0 ± 0.3[c]	6.4 ± 0.1 7.3 ± 0.2[b] 14.3 ± 0.3[c]		

[a] Reactions were conducted in 100 mM potassium phosphate buffer, pH 8.0. Unless otherwise noted, reductive half-reaction parameters were determined based on global analysis of diode array data, as described in the text. Steady-state kinetic parameters were previously reported by Wagner and Jorns (3).

[b] Determined based on spectra calculated for the MSOX·sarcosine complex at various substrate concentrations, as described in the text.

[c] Determined based on the observed rate of disappearance of the MSOX·sarcosine charge transfer complex, as monitored at 516 nm with the stopped flow in photomultiplier mode.

Table 2

Kinetic parameters for formation of charge transfer complexes with MSOX and substrate or an inhibitor[a]

	complex	
	MSOX·sarcosine	**MSOX·MTA**
k_2/k_1 (mM)	29 ± 4	87 ± 8
k_3 (s^{-1})	1010 ± 40	2450 ± 150
k_4 (s^{-1})	190 ± 20	18 ± 5
$K_{d\ (macroscopic)}$ (mM)	4.6 ± 0.3 (calc) 6.4 ± 0.1 (obs)[b]	0.63 ± 0.08 (calc) 0.50 ± 0.02 (obs)[c]

[a] Reactions were conducted in 100 mM potassium phosphate buffer, pH 8.0, at 5 °C. The observed rate of charge transfer complex formation at various concentrations of sarcosine or MTA (k_{obs}) was determined by analysis of absorbance changes at 516 nm or 532 nm, respectively. Values for k_2/k_1, k_3 and k_4 were obtained based on the fit of the data (k_{obs}) to equation 2 and used to calculate values for the macroscopic K_d, as described in the text.

[b] Determined based on reduction rates estimated by global analysis of diode array data at various sarcosine concentrations in 100 mM potassium phosphate buffer, pH 8.0, at 5 °C.

[c] Determined in a static spectrophotometric titration of MSOX with MTA in 100 mM potassium phosphate buffer, pH 8.0, at 5 °C.